

Vanadium Docked Covalent-Organic Frameworks: An Effective Heterogeneous Catalyst for Modified Mannich-Type Reaction

Harsh Vardhan,[†] Linxiao Hou,[†] Eaindra Yee,[†] Ayman Nafady,[‡] Mohammed A. Al-Abdrabalnabi,[‡] Abdullah M. Al-Enizi,^{*,‡} Yanxiong Pan,[§] Zhongyu Yang,[§] and Shengqian Ma^{*,†}

[†]Department of Chemistry, University of South Florida, 4202 East Fowler Avenue, Tampa, Florida 33620, United States

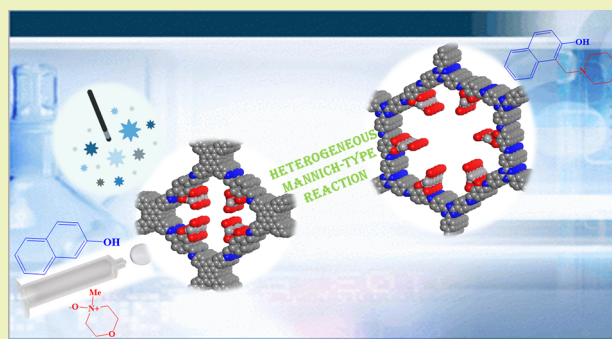
[‡]Department of Chemistry, College of Science, King Saud University, Riyadh 11451, Saudi Arabia

[§]Department of Chemistry & Biochemistry, North Dakota State University, 1231 Albrecht Boulevard, Fargo, North Dakota 58108, United States

Supporting Information

ABSTRACT: Accurate and precise control of the transition-metal ions in the docking sites of porous functional materials especially covalent-organic frameworks (COFs) is a challenging task in the synthesis of hybrid materials. In this work, we demonstrate the successful synthesis, characterization, and utilization of two stable vanadium docked COFs, namely VO-TAPT-2,3-DHTA and VO-PyTTA-2,3-DHTA as efficient heterogeneous catalysts for Mannich-type reactions. The obtained results revealed that the as-prepared vanadium-decorated COFs are robust and maintain framework crystallinity, reusability, and efficiency under the sway of electronic and steric effects. Significantly, this work opens up the opportunity for docking other metals and exploring practically and industrially important catalytic reactions.

KEYWORDS: Covalent-organic frameworks, Postsynthetic modification, Heterogeneous catalysis, Mannich reaction, Vanadium catalyst



INTRODUCTION

The Mannich reaction is one of the most vital carbon–carbon bond forming reactions widely used by organic chemist in the synthesis of aminocarbonyl compounds (Mannich base) and has attracted a great deal of attention since its discovery in the early 20th century.^{1–4} The diversity of this reaction is rapidly growing in the field of synthetic organic chemistry due to various reasons,^{5–16} first, it withstands a range of functional groups; second, it offers a robust way for the preparation of aminocarbonyl and several other derivatives; and last, it is useful in the synthesis of medicinally important materials such as β -lactams, α - and γ -amino alcohols, α - and β -amino acid derivatives, peroxy acetylenic alcohols, and others. Despite its significant synthetic worth, the Mannich reaction is confronted with a number of serious shortcomings such as the formation of undesired side products and inability to control stereo- and regioselectivity.^{17–19} To overcome the drawbacks, imines and iminium salts, chiral auxiliaries and chiral catalysts, basic nanocrystalline magnesium oxide, copper nanoparticles, poly-(amidoamine) and others have been developed and extensively used.^{20–24}

Mechanistically, this reaction comprises the addition of a carbon nucleophile to an iminium ion to form secondary or tertiary derivatives liable on the nature of the substrates. Among

the various methods reported for the formation of iminium ions,^{25–28} the most commonly used approach is Polonovsky or modified Polonovsky reaction in which tertiary amine oxide is reacted with a promoter such as SO_2 , $(\text{CH}_3\text{CO})_2\text{O}$, and $(\text{CF}_3\text{CO})_2\text{O}$ as shown in **Scheme 1**. These promoters are difficult to handle and used in excess amounts to facilitate the reaction. In contrast, vanadium facilitated reactions are feasible and afford excellent yield, depending on the vanadium source (V_2O_5 , $\text{VO}(\text{acac})_2$, $\text{VO}(\text{SO}_4)\cdot 2\text{H}_2\text{O}$).²⁹ Furthermore, the synthesis of safe, effective, recyclable and reusable new catalysts would be of great importance from an application point of view. Within this context, burgeoning classes of porous functional materials, such as metal–organic frameworks (MOFs), covalent-organic frameworks (COFs), porous organic polymers (POPs) synthesized under the principle of reticular chemistry are of escalating interest.

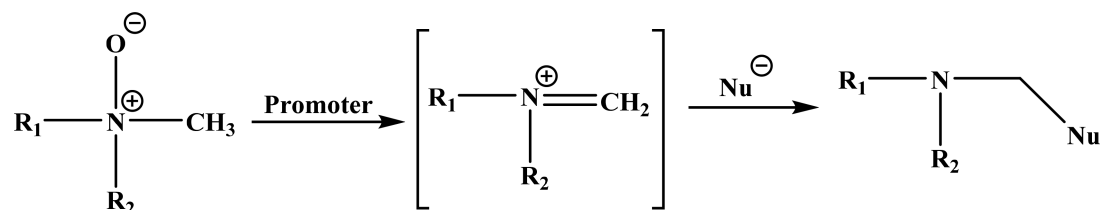
Of particular relevance to the present paper, COFs, which represent a new class of porous crystalline materials built by strong covalent bonds in a periodic arrangement from lighter elements (C, H, B, N, O), have attracted enormous attention

Received: October 17, 2018

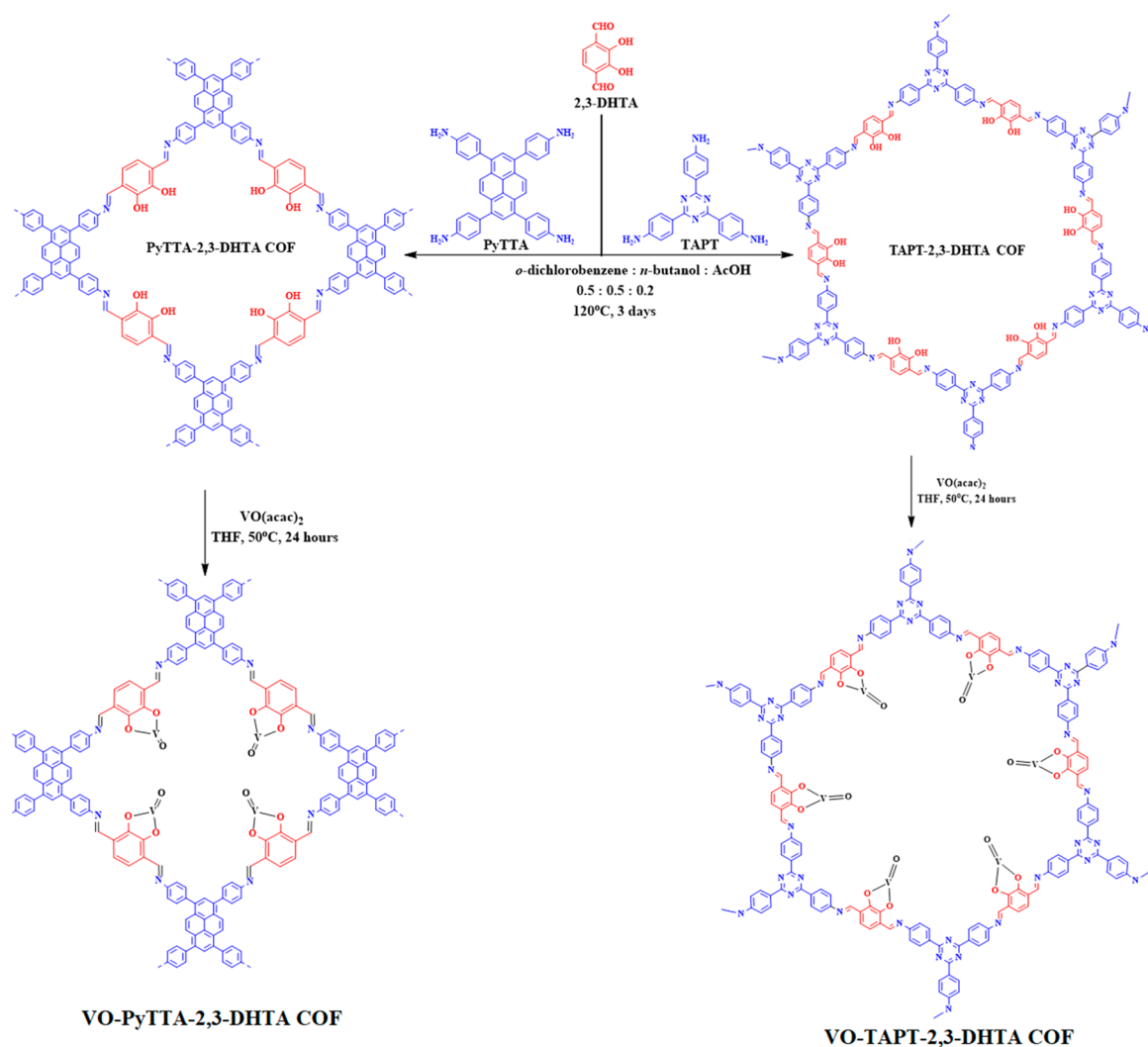
Revised: December 26, 2018

Published: February 11, 2019

Scheme 1. Synthesis of Iminium Ions Using Promoter (Polonovsky Reaction)



Promoter = Ac_2O , TFAA, SO_2 .

Scheme 2. Schematic Representation of 2D TAPT-2,3-DHTA COF, PyTTA-2,3-DHTA COF, and Vanadium Docked VO-TAPT-2,3-DHTA COF, ⁸⁹ VO-PyTTA-2,3-DHTA COF Synthesis

due to structural versatility, high porosity, low density, and excellent chemical and thermal stability.^{30–48} These fascinating properties make COFs not only a new area of materials research in recent years, but also an outstanding candidate for a plethora of applications related to catalysis,^{49–61} gas storage/separation,^{62–67} environmental remediation,^{68,69} optoelectronics,^{70–72} and others.^{73–86} Importantly, COFs with imine or hydrazone linkage are stable in air and in various protic or aprotic solvents, whereas, boronate ester linkage or boroxines framework are unstable in the same environment. Moreover, postsynthetic chemical modification of COFs or docking with

various transition metal ions opens up enormous opportunities in materials science and engineering.^{87,88} In this contribution, successful employment of highly stable vanadium-docked COFs (VO-TAPT-2,3-DHTA⁸⁹ and VO-PyTTA-2,3-DHTA) is presented as a promising and efficient heterogeneous catalyst for a Mannich-type reaction with superior catalytic activity, recyclability, and retainment of crystallinity.

EXPERIMENTAL SECTION

Materials. All solvents and deuterated solvents were purchased from commercial sources and used as received without any further

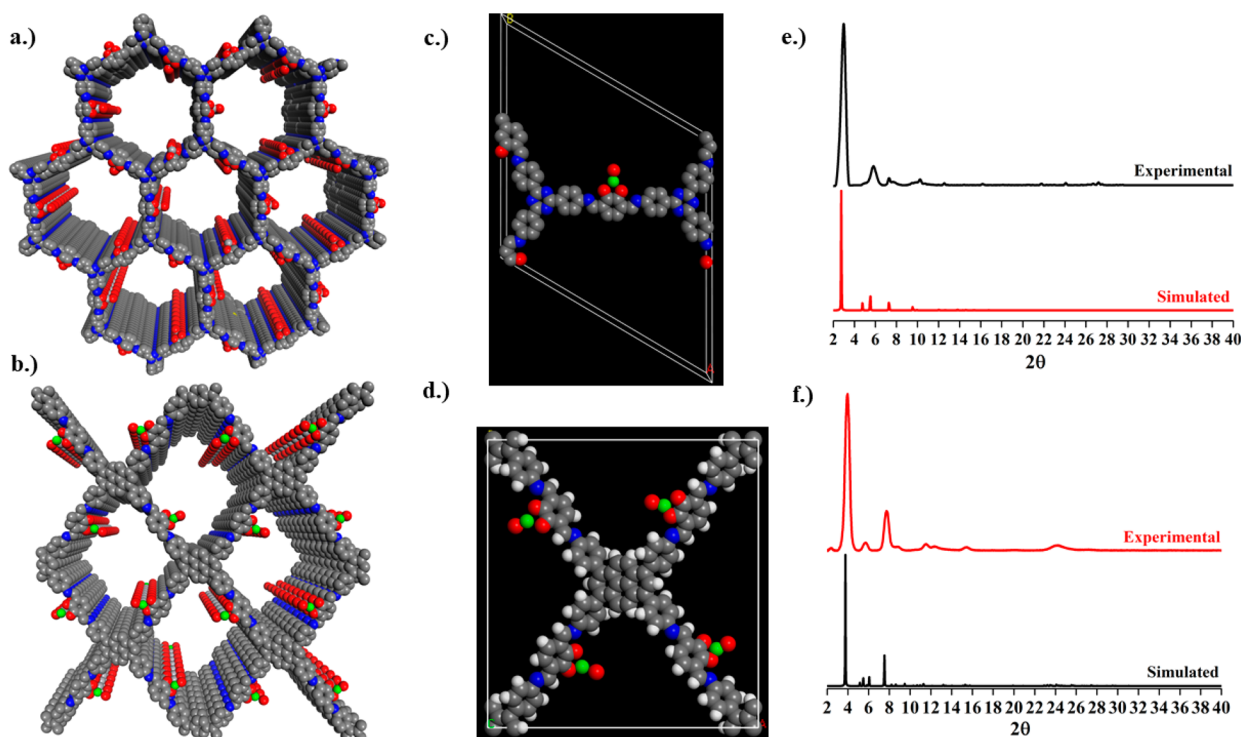


Figure 1. Graphic extended view of the stacking structure: (a) VO-TAPT-2,3-DHTA COF; (b) VO-PyTTA-2,3-DHTA COF. Unit cell of (c) VO-TAPT-2,3-DHTA COF; (d) VO-PyTTA-2,3-DHTA COF. Comparison of experimental and simulated PXRD pattern of (e) VO-TAPT-2,3-DHTA COF; (f) VO-PyTTA-2,3-DHTA COF.

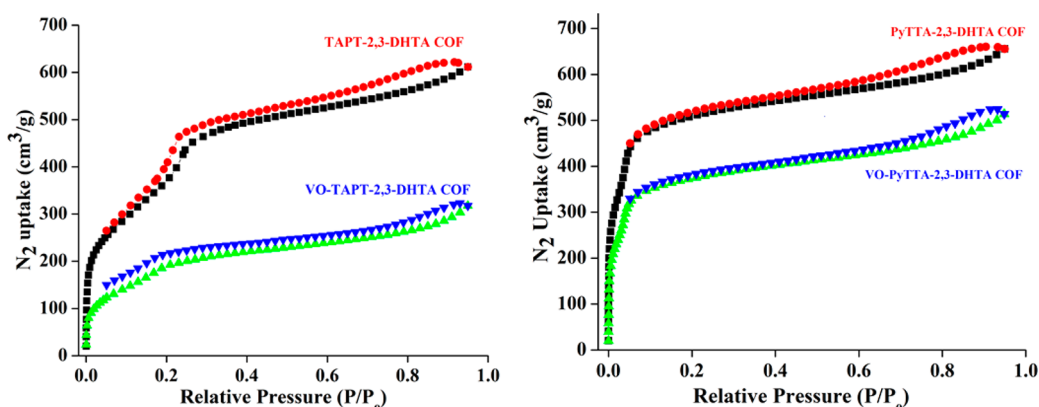


Figure 2. N_2 sorption isotherms comparison of TAPT-2,3-DHTA/VO-TAPT-2,3-DHTA COF (left) and PyTTA-2,3-DHTA/VO-PyTTA-2,3-DHTA COF (right).

purification. 4-Aminobenzonitrile (Matrix Scientific, 98%), trifluoromethanesulfonic acid (Acros Organics, 99%), 4-(4,4,5,5-tetramethyl-1,3,2-dioxaborolan-2-yl)aniline (Oakwood products, 98%), palladium tetrakis(triphenyl phosphine) (Sigma-Aldrich, 99%), potassium carbonate (Sigma-Aldrich, 99%), sodium acetate (Sigma-Aldrich, 99%), hydrochloric acid (Sigma-Aldrich, ACS grade), veratrole (Acros Organics, 98%), catechol (Alfa Aesar, 99%), vanadyl sulfate (Bio Medical), *n*-butyllithium solution (Aldrich), boron tribromide (Acros Organics, 99%), trimethyl amine *N*-oxide (Aldrich, 98%), vanadyl acetylacetonate (Alfa Aesar, 97%), ammonium chloride (Sigma-Aldrich, $\geq 99.8\%$), chloroform (Fischer chemical), ethyl acetate (Sigma-Aldrich, $\geq 99.8\%$), tetrahydrofuran (Acros Organics, 99%), and dimethylformamide (Sigma-Aldrich, $\geq 99.8\%$) were used as received. $K_2[VO(\text{catechol})_2]$,⁹⁰ 2,3-dihydroxyterephthalaldehyde (2,3-DHTA),⁹¹ 4,4',4'',4'''-(pyrene-1,3,6,8-tetrayl) tetraaniline (PyTTA),⁹² and 1,3,5-tris(4-aminophenyl) triazine (TAPT)⁹³ were synthesized according to previously reported procedures.

Synthesis of TAPT-2,3-DHTA COF. TAPT-2,3-DHTA COF was prepared as per the previously reported procedure.⁹⁴ A Pyrex tube measuring o.d. \times i.d. = $9.5 \times 7.5 \text{ mm}^2$ was charged with 2,3-dihydroxy terephthalaldehyde (7.5 mg, 0.045 mmol) and 1,3,5-tris(4-aminophenyl) triazine (10.6 mg, 0.03 mmol) in 1.2 mL of a 5:5:2 v:v solution of *o*-dichlorobenzene/*n*-butanol/3 M aqueous acetic acid. The tube was flash frozen at 77 K (liquid N_2 bath) evacuated and flame-sealed. The reaction mixture was heated at 120 °C for 3 days to afford a red precipitate which was isolated by filtration and washed with dry tetrahydrofuran and dry acetone. The fluffy powder was dried at 120 °C under vacuum for 12 h before it was subjected to any characterization.

Synthesis of PyTTA-2,3-DHTA COF. PyTTA-2,3-DHTA COF was prepared as per the previously reported procedure.⁹⁵ A Pyrex tube measuring o.d. \times i.d. = $9.5 \times 7.5 \text{ mm}^2$ was charged with 2,3-dihydroxy terephthalaldehyde (6.6 mg, 0.04 mmol) and 4',4'',4''',4-(pyrene-1,3,6,8-tetrayl) tetraaniline (11.3 mg, 0.02 mmol) in 1.2 mL of a 5:5:2 v:v solution of *o*-dichlorobenzene/*n*-butanol/3 M aqueous acetic acid.

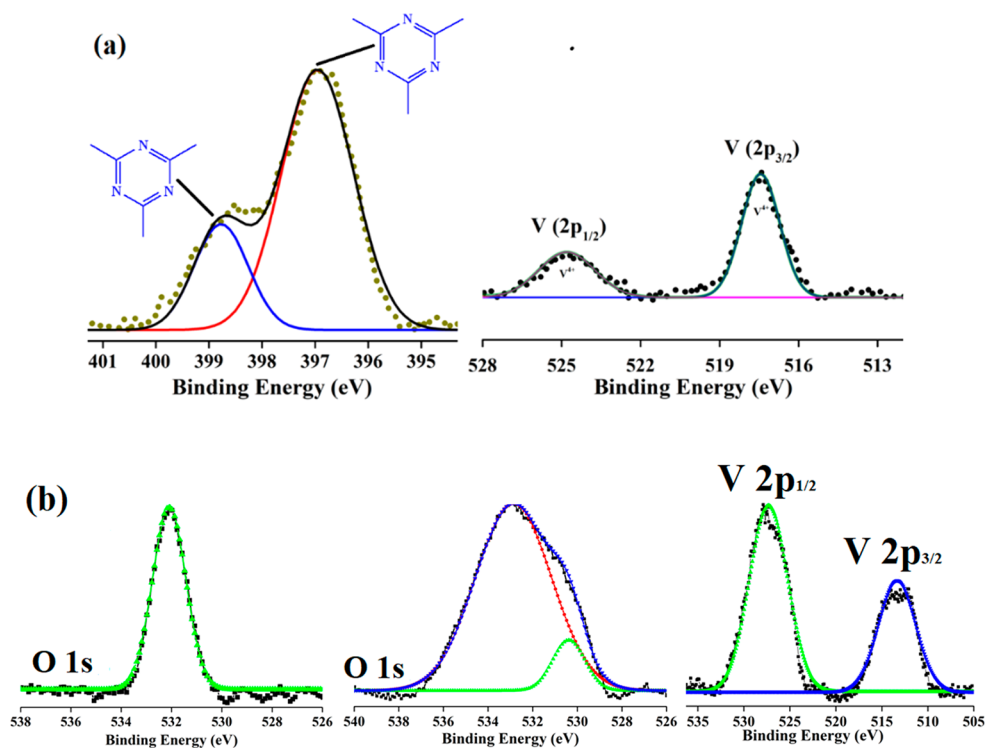


Figure 3. XPS spectra of (a) VO-TAPT-2,3-DHTA COF; nitrogen (left) and vanadium (right). (b) PyTTA-2,3-DHTA COF; oxygen (left), VO-PyTTA-2,3-DHTA COF; oxygen (middle) and vanadium (right).

The tube was flash frozen at 77 K (liquid N₂ bath) evacuated and flame-sealed. The reaction mixture was heated at 120 °C for 3 days to afford a dark red precipitate which was isolated by filtration and washed with dry tetrahydrofuran and dry acetone. The fluffy red powder was dried at 120 °C under vacuum for 12 h.

Synthesis of VO-TAPT-2,3-DHTA COF. To the 25 mL Schlenk tube, as-synthesized TAPT-2,3-DHTA COF (10 mg) was added into a solution of VO(acac)₂ (61 mg) in THF (15 mL). The reaction mixture was heated at 50 °C in an oil bath under an inert atmosphere for 24 h. The precipitate so formed was centrifuged and washed with anhydrous THF and then with dry acetone to remove any excess metal ions. The product was dried under vacuum for 12 h before being subjected to any characterization.⁸⁹

A similar procedure was used to synthesize VO-PyTTA-2,3-DHTA COF except the amount and volume of VO(acac)₂ (55 mg) and THF (10 mL).

Catalytic Tests. In a typical procedure for the Mannich-type reaction, alcohol (1 mmol), NMO (1.2 mmol), and VO-TAPT-2,3-DHTA or VO-PyTTA-2,3-DHTA COFs (35 mg) in anhydrous CH₂Cl₂ (5 mL) was continuously stirred in a 10 mL Schlenk tube at 40 °C under inert atmosphere for 12 h. At the end of the reaction, the catalyst was separated and the filtrate was evaporated under vacuum to dryness to form a Mannich base in a quantitative yield. In a few cases, column chromatography was used to obtain pure product.

Recyclability Examination of VO-TAPT-2,3-DHTA COF/VO-PyTTA-2,3-DHTA COF. The catalyst was separated after the Mannich-type reaction was washed with anhydrous CH₂Cl₂, THF, acetone, and dried overnight at 80 °C under vacuum. Later, the catalyst was reused for the next Mannich-type reaction under the same reaction conditions. This procedure was repeated at least five times to inspect the recyclability of vanadium decorated COFs.

RESULTS AND DISCUSSION

The two-dimensional imine-linked TAPT-2,3-DHTA and PyTTA-2,3-DHTA COFs bearing hydroxyl functionalities were successfully synthesized by the reaction of 1,3,5-tris(4-aminophenyl) triazine (TAPT)/4,4',4'',4'''-(pyrene-1,3,6,8-

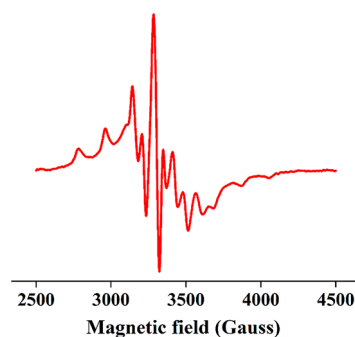
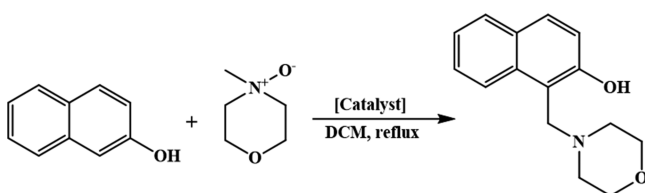


Figure 4. EPR spectra of VO-TAPT-2,3-DHTA COF.

tetrayl)tetraaniline (PyTTA) and 2,3-dihydroxy terephthalaldehyde (2,3-DHTA) in the presence of 3 M acetic acid according to the previously reported procedure^{94,95} as shown in Scheme 2. Powder X-ray diffraction patterns (PXRD) confirmed the crystalline nature of both porous frameworks. TAPT-2,3-DHTA COF exhibited an intense peak at 2.8° along with few minor peaks at 4.9°, 5.9°, 7.6°, 10.1° and 23.2° attributed to the (100), (110), (200), (120), (220), and (001) facets respectively with P1 space group (Figure S2), whereas PyTTA-2,3-DHTA COF displayed diffraction peaks at 3.8°, 5.6°, 7.6°, 8.7°, 11.6°, 12.4°, 15.5°, 23.9°, which are ascribed to (110), (020), (220), (030), (040), (240), (440) and (001) facets, respectively (Figure S3), with PMM2 space group. The simulated PXRD patterns of both frameworks show a good match with experimental ones, and an extraordinary high crystallinity of frameworks arose from the strong intramolecular hydrogen bonding between the imine nitrogen and hydroxyl group of aldehydes which in turn, kept the phenyl rings in one plane and facilitated stacking interaction between the layers. The Fourier-transform infrared (FT-IR) analysis of both

Table 1. Role of Different Catalysts and Conditions for Preliminary Mannich-Type Reaction^a

no.	catalyst	solvent	temp (°C)	time (h)	% yield
1 ^b	VOSO ₄ ·2H ₂ O	DCM	40	12	49
2 ^b	VO(acac) ₂	DCM	40	12	91
3 ^b	VO(catechol) ₂	DCM	40	12	89
4	TAPT-2,3-DHTA COF	DCM	40	12	<5
5	PyTTA-2,3-DHTA COF	DCM	40	12	<5
6	VO-TAPT-2,3-DHTA COF	DCM	40	12	98
7	VO-PyTTA-2,3-DHTA COF	DCM	40	12	96
8	reused VO-TAPT-2,3-DHTA COF	DCM	40	12	96
9	reused VO-PyTTA-2,3-DHTA COF	DCM	40	12	98

^aReaction conditions: β -Naphthol (1.0 mmol), NMO (1.2 mmol).

^bCatalyst (10 mol %); {(VO-TAPT-2,3-DHTA COF = 35 mg, containing 0.034 mmol of vanadium); (VO-PyTTA-2,3-DHTA COF = 35 mg, containing 0.027 mmol of vanadium)} and DCM = 5 mL.

TAPT-2,3-DHTA and PyTTA-2,3-DHTA COFs showed the disappearance of the $\text{C}=\text{O}$ stretching vibrational band at 1680 cm^{-1} and the appearance of the $\text{C}=\text{N}$ stretching vibration peak at 1618 cm^{-1} as shown in Figure S4–5, further confirming the dynamic imine condensation reaction between aldehyde and amines. Thermogravimetric analysis (TGA) showed high thermal stability with a breakdown temperature at $450\text{ }^\circ\text{C}$ (Figure S6,7), suggesting the maintenance of framework crystallinity at elevated temperatures. To further support this thermostability, a variable temperature PXRD (VT-PXRD) pattern at higher temperatures showed complete retention of major and minor peaks as shown in Figures S8 and S9. Moreover, the chemical structure of TAPT-2,3-DHTA and PyTTA-2,3-DHTA COFs were affirmed by ^{13}C cross polarized magic angle spinning (CP-MAS) solid state NMR spectrum. The complete consumption of 2,3-DHTA was ascribed to the absence of a formyl group signal at $\sim 190\text{ ppm}$, whereas the imine linked carbon at $\sim 160\text{ ppm}$ established the condensation reaction between aldehyde and amine as shown in Figures S10 and S11. The porosity of both COFs was measured by nitrogen sorption isotherms at 77 K. The Brunauer–Emmett–Teller (BET), Langmuir surface area, and pore size (nonlocal density functional theory) of TAPT-2,3-DHTA and PyTTA-2,3-DHTA COFs are $1151\text{ m}^2\text{ g}^{-1}$, $1490\text{ m}^2\text{ g}^{-1}$, 3.0 nm and $1892\text{ m}^2\text{ g}^{-1}$, $2345\text{ m}^2\text{ g}^{-1}$, 1.6 nm respectively (Figure 2, Figures S12 and S13). Moreover, the adsorption maxima of CO_2 uptake at 1 bar and 298 K is $38\text{ cm}^3\text{ g}^{-1}$ and $35\text{ cm}^3\text{ g}^{-1}$ for TAPT-2,3-DHTA and PyTTA-2,3-DHTA COFs, respectively, (Figures S14 and S15).

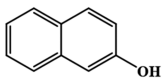
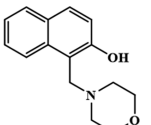
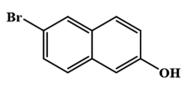
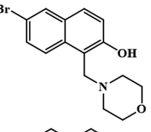
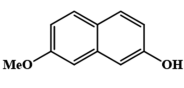
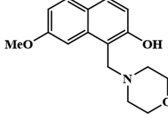
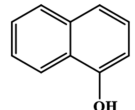
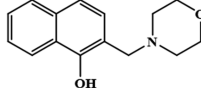
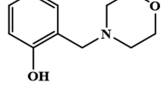
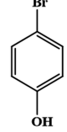
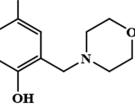
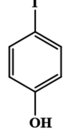
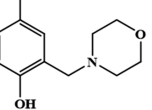
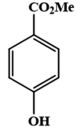
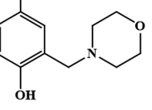
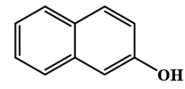
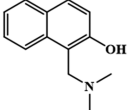
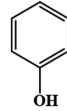
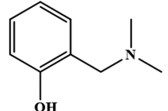
Encouraged by the high crystallinity and the presence of hydroxyl functionality in both porous frameworks, dark brown colored vanadium-docked frameworks, denoted as VO-TAPT-2,3-DHTA and VO-PyTTA-2,3-DHTA, were prepared by the single step reaction of TAPT-2,3-DHTA/PyTTA-2,3-DHTA with VO(acac)₂ at $50\text{ }^\circ\text{C}$ for 24 h (Scheme 2). With vanadium-functionalization in hand, the PXRD patterns revealed that VO-

TAPT-2,3-DHTA and VO-PyTTA-2,3-DHTA COFs with different vanadium content retained characteristic diffraction peaks at 2.8° and 3.8° , respectively, thereby indicating that the structural crystallinity of COFs had been well-maintained during postsynthetic modification. The experimental PXRD patterns of both modified frameworks match well with the simulated patterns (Figure 1e,f). This structural retainment during different chemical or metal modifications in various 2D and 3D COFs was also observed by different research groups including ours as well.^{96–98} The successful grafting of vanadium moieties in porous frameworks was further confirmed by elemental analysis (Table S1), FT-IR spectra, which showed an intense $\text{C}=\text{N}$ stretching vibration band at $\sim 1620\text{ cm}^{-1}$ along with $\text{V}=\text{O}$ functionalities at $\sim 970\text{ cm}^{-1}$ (Figure S16 and S17). Given the high thermal stability (up to $400\text{ }^\circ\text{C}$) of VO-TAPT-2,3-DHTA and VO-PyTTA-2,3-DHTA COFs as shown by TGA (Figure S18–19), this class of vanadium-based frameworks can be used as potential heterogeneous catalysts at room or higher temperature. To investigate the porosity of VO-TAPT-2,3-DHTA and VO-PyTTA-2,3-DHTA COFs, nitrogen sorption isotherms at 77 K were collected. The BET, Langmuir surface area and pore size (nonlocal density functional theory) of VO-TAPT-2,3-DHTA and VO-PyTTA-2,3-DHTA is $562\text{ m}^2\text{ g}^{-1}$, $750\text{ m}^2\text{ g}^{-1}$, 2.5 nm and $1382\text{ m}^2\text{ g}^{-1}$, $1714\text{ m}^2\text{ g}^{-1}$, 1.5 nm , respectively (Figure 2, Figures S20 and S21). The substantial reduction in surface area and pore size is possibly due to partial impasse of framework channel by incorporation of vanadium moieties in the parent TAPT-2,3-DHTA and PyTTA-2,3-DHTA frameworks.

To understand the deeper insight of vanadium docking condition in the modified frameworks, X-ray photoelectron spectroscopy (XPS) was conducted. XPS spectra of pristine TAPT-2,3-DHTA, PyTTA-2,3-DHTA, and modified VO-TAPT-2,3-DHTA, VO-PyTTA-2,3-DHTA COFs were analyzed. The N 1s spectra of VO-TAPT-2,3-DHTA showed two different peaks at 397 and 399 eV, the same as pristine TAPT-2,3-DHTA, which can be assigned to the triazine units underlining the absence of any coordination with triazine nitrogen (Figure 3a). Moreover, O 1s spectra showed an additional peak at 529 eV assignable to the $\text{V}=\text{O}$ bond present in the VO-TAPT-2,3-DHTA. To identify the oxidation state of vanadium, the XPS spectra of V 2p region in the VO-TAPT-2,3-DHTA highlighted the binding energy of V $2p_{1/2}$ and V $2p_{3/2}$ at 524 and 517 eV, respectively, which in turn indicated the presence of V(IV) in the modified framework (Figure 3a). A similar observation was also noted for the O 1s and V 2p region in the VO-PyTTA-2,3-DHTA as presented in Figure 3b. The O 1s spectra of pristine PyTTA-2,3-DHTA showed only one peak (C–O) at 534 eV, whereas VO-PyTTA-2,3-DHTA exhibited a slight shift along with extra peaks at 532.6 and 530 eV, respectively, corresponding to the oxygen binding with vanadium and $\text{V}=\text{O}$ bond present in the modified heterogeneous catalyst. The fact that the V 2p region contained two distinct peaks of V $2p_{1/2}$ and V $2p_{3/2}$ at 526 and 514 eV, respectively, revealed the presence of V^{4+} .

To further support the presence of V^{4+} , electron paramagnetic resonance (EPR) spectroscopy of VO-TAPT-2,3-DHTA COF was conducted. The EPR spectrum exhibited a characteristic of V(IV) with an axial pattern as shown in Figure 4. Maurya and co-workers also reported similar observation for polymer anchored vanadium complex.⁹⁹ The vanadium content of VO-TAPT-2,3-DHTA and VO-PyTTA-2,3-DHTA COFs was measured to be 4.9 and 3.8 wt %, respectively, by

Table 2. Mannich-Type Reaction with Differently Substituted Substrates Catalyzed by VO-TAPT-2,3-DHTA and VO-PyTTA-2,3-DHTA COFs^a

Entry	Substituted Alcohol	Amine <i>N</i> -Oxide	Time (h)	Product	% Yield	
					VO-TAPT-2,3-DHTA	VO-PyTTA-2,3-DHTA
1		NMO	12		98	96
2		NMO	12		99	99
3		NMO	12		99	97
4		NMO	12		91	87
5		NMO	12		77	71
6		NMO	12		88	82
7		NMO	12		85	81
8		NMO	12		98	95
9		TMNO	24		88	83
10		TMNO	24		92	89

^aReaction conditions: substituted alcohol (1.0 mmol), amine *N*-oxide (1.2 mmol), {(VO-TAPT-2,3-DHTA COF = 35 mg, containing 0.034 mmol of vanadium); (VO-PyTTA-2,3-DHTA COF = 35 mg, containing 0.027 mmol of vanadium)}; DCM = 5 mL; temperature = 40 °C; NMO = *N*-methylmorpholine *N*-oxide; TMNO = trimethylamine *N*-oxide.

inductively coupled plasma mass spectrometry (ICP-MS). Additionally, scanning electronic microscopy (SEM), and transmission electronic microscopy (TEM) revealed that modified VO-TAPT-2,3-DHTA and VO-PyTTA-2,3-DHTA

COFs showed petal or flake-like morphologies similar to the parent frameworks (Figures S23 and S24). SEM-EDS mapping revealed uniform distributions of the C, N, O, V elements in the modified frameworks (Figure S23 and S24) thereby implying

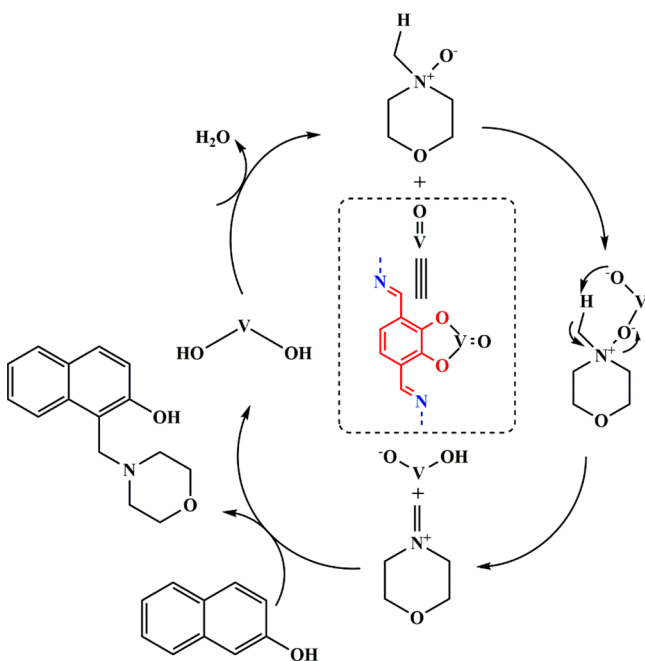


Figure 5. Proposed mechanism of Mannich-type reaction catalyzed by vanadium modified frameworks (VO-TAPT-2,3-DHTA COF and VO-PyTTA-2,3-DHTA COF).

that a postsynthetic modification has occurred evenly throughout the porous frameworks.

After determining the porosity, stability, and high density of vanadium docked frameworks, the role of VO-TAPT-2,3-DHTA and VO-PyTTA-2,3-DHTA as new heterogeneous catalysts for Mannich-type reaction was undertaken. In doing so, the stability of vanadium modified frameworks in DCM as a solvent was investigated using both PXRD and FT-IR as illustrated in Figures S25 and S26. In a preliminary screening, a Mannich-type reaction of β -naphthol and 4-methylmorpholine *N*-oxide (NMO) was carried out in DCM at 40 °C for 12 h using $\text{VOSO}_4 \cdot 2\text{H}_2\text{O}$, $\text{VO}(\text{acac})_2$, $\text{VO}(\text{catechol})_2$, TAPT-2,3-DHTA, PyTTA-2,3-DHTA, VO-TAPT-2,3-DHTA, and VO-PyTTA-2,3-DHTA as catalysts (Table 1). Virtually, $\text{VOSO}_4 \cdot 2\text{H}_2\text{O}$, as well as TAPT-2,3-DHTA and PyTTA-2,3-DHTA COFs showed poor catalytic performance (Table 1, entries 1, 4, 5), whereas $\text{VO}(\text{acac})_2$, $\text{VO}(\text{catechol})_2$, VO-TAPT-2,3-DHTA, and VO-PyTTA-2,3-DHTA COFs almost gave rise to quantitative yield of the major product (Table 1, entries 2, 3, 6, 7).¹⁰⁰ In spite of the high percentage yield (91%) that was

obtained when $\text{VO}(\text{acac})_2$ is used as a catalyst (Scheme 1), it exhibited poor catalytic efficiency for a variety of other substrates such as phenol and substituted naphthol derivatives. Practically, the difficulty in the separation of $\text{VO}(\text{acac})_2$ catalyst along with the excess production of vanadium waste profoundly limited its utilization. In contrast, because VO-TAPT-2,3-DHTA and VO-PyTTA-2,3-DHTA are heterogeneous catalysts, the probability of deactivation during the reaction of phenol or substituted naphthol with NMO is reduced. This enables recyclability, minimal waste, and easy separation of the catalyst.

This remarkable catalytic efficacy of our VO-based COFs prompted us to examine a range of substrates under steric and electronic influence as illustrated in Table 2. Significant catalytic conversion had been achieved for almost all the substrates used. In contrast, the $\text{VO}(\text{acac})_2$ homogeneous system showed less than 75% yield for products 2 and 3, and less than 40% yield for product 5, even after longer reaction time. It is noteworthy that these heterogeneous catalytic systems are broadly applicable and showed tolerance to a variety of electron donating or electron withdrawing substituents on the aromatic ring. This excellent catalytic activity can be ascribed to various reasons such as robustness of frameworks, large surface area, pore volume, ingress of substrate and egress of product and more importantly, the presence of coordinating sites in the parent framework.

After detailed study of the modified Mannich-type reaction, a plausible mechanism was proposed to explain the step-by-step conversion to Mannich base. First, active vanadium centers ($\text{V}=\text{O}$) of VO-TAPT-2,3-DHTA and VO-PyTTA-2,3-DHTA COFs are coordinated to 4-methylmorpholine *N*-oxide (NMO), followed by an intramolecular elimination thereby promoting a six-membered transition intermediate structure that results in the formation of iminium ions. Second, $[\text{V}(\text{OH})(\text{O}^-)]$ abstracts acidic proton from β -naphthol to create a negatively charged oxygen species which in turn, generates acidic carbon that afterward reacts with iminium ions to form a Mannich-base. Lastly, a water molecule is eliminated from $[\text{V}(\text{OH})_2]$ allowing for regeneration of vanadium-docked catalyst as shown in Figure 5.

Recyclability and stability are some key traits of catalysts to be considered for a large-scale industrial application. In this regard, we found that VO-TAPT-2,3-DHTA and VO-PyTTA-2,3-DHTA can be recovered by filtration after completion of the catalytic reaction, followed by extensive wash with copious amount of dichloromethane and tetrahydrofuran before being used for the next catalytic reaction. The percentage yield of

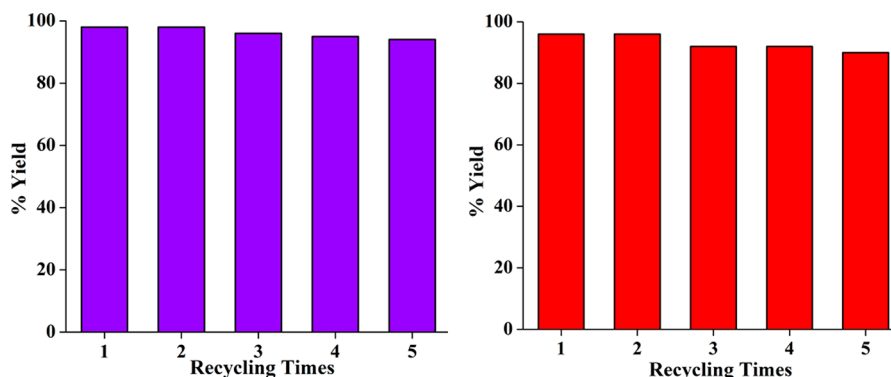


Figure 6. Recycling test of VO-TAPT-2,3-DHTA COF (left) and VO-PyTTA-2,3-DHTA COF (right) catalysts for Mannich-type reaction.

Mannich base, structure (1) in Table 2 for five repeated runs is shown in Figure 6. No significant difference in percentage yield of product is observed, thereby implying the excellent recyclability of vanadium-docked frameworks. In addition, the turn over frequency (TOF) for both vanadium docked heterogeneous catalyst up to five catalytic cycles is shown in Table S4. The recovered VO-TAPT-2,3-DHTA and VO-PyTTA-2,3-DHTA catalysts were exposed to physio-chemical analysis such as PXRD, FT-IR, SEM, and TEM in order to establish the crystallinity, and the presence of $-C=N$ linkage together with probing any changes in morphology. The comparative PXRD patterns of pristine VO-TAPT-2,3-DHTA, VO-PyTTA-2,3-DHTA, and the recovered catalysts after finishing the last catalytic cycle (Figure S28), confirmed the structural integrity of both VO-TAPT-2,3-DHTA and VO-PyTTA-2,3-DHTA. FT-IR spectra of the recovered vanadium-docked heterogeneous catalysts showed the $-C=N$ stretching vibration at $\sim 1619\text{ cm}^{-1}$ representing the complete retention of imine linkage ($C=N$) without any change in the structure of vanadium-modified frameworks after five successive runs (Figure S29). The vanadium content of recyclable VO-TAPT-2,3-DHTA and VO-PyTTA-2,3-DHTA COFs catalyst after the last catalytic cycle are comparable to pristine docked frameworks, thereby, discarding any possibility of vanadium leaching. Moreover, SEM and TEM images (Figure S30) of the recycled catalysts showed similar morphology as those of pristine frameworks, which further supports the successful reuse of these heterogeneous catalysts for a modified Mannich-type reaction. Taken together, the overall finding of this work clearly demonstrates that the incorporation of vanadium moieties in COFs as a promising strategy for utilization of these porous materials and others as a potent heterogeneous catalyst for Mannich-type as well as various key organic transformations and name reactions.^{101–107}

CONCLUSIONS

We have successfully explored the potent role of two vanadium-docked COFs (VO-TAPT-2,3-DHTA and VO-PyTTA-2,3-DHTA) as efficient and effective heterogeneous catalysts for the Mannich-type reaction. These porous vanadium catalysts can be utilized for a wide range of substrates, including electron donating and/or electron withdrawing substituents, and can easily be recycled and reused for many times without any loss of structural integrity, stability, and activity. The catalysis protocol envisaged in this study can be applicable to other important named reactions as well as the docking of other transition metals for various organic and organometallic catalytic reactions.

ASSOCIATED CONTENT

Supporting Information

The Supporting Information is available free of charge on the ACS Publications website at DOI: 10.1021/acssuschemeng.8b05373.

Materials and methods; NMR spectra; PXRD patterns; FTIR; TGA curves; SEM images; fractional atomic coordinates of COFs; other data as described in the text (PDF)

AUTHOR INFORMATION

Corresponding Authors

*E-mail: sqma@usf.edu.

*E-mail: amenizi@ksu.edu.sa.

ORCID

Zhongyu Yang: 0000-0002-3018-3608

Shengqian Ma: 0000-0002-1897-7069

Notes

The authors declare no competing financial interest.

ACKNOWLEDGMENTS

The authors acknowledge University of South Florida (USF) for support of this work. The authors also extend their sincere appreciation to the Deanship of Scientific Research at King Saud University for partially funding this Research Group (RG-1435-010). X-ray photoelectron spectroscopy studies were carried in the Nebraska Nanoscale Facility, Nebraska Center for Materials and Nanoscience, which is supported by the NSF under Award NNCI 1542182, and the Nebraska Research Initiative (NRI).

REFERENCES

- (1) Mannich, C.; Krösche, W. Ueber ein Kondensationsprodukt aus Formaldehyd, Ammoniak und Antipyrin. *Arch. Pharm.* **1912**, *250*, 647–667.
- (2) Arend, M.; Westermann, B.; Risch, N. Moderne Varianten der Mannich-Reaktion. *Angew. Chem.* **1998**, *110*, 1096–1122.
- (3) Notz, W.; Tanaka, F.; Barbas, C. F., III Enamine-Based Organocatalysis with Proline and Diamines: The Development of Direct Catalytic Asymmetric Aldol, Mannich, Michael, and Diels-Alder Reaction. *Acc. Chem. Res.* **2004**, *37* (8), 580–591.
- (4) Kobayashi, S.; Mori, Y.; Fossey, J. S.; Salter, M. M. Catalytic Enantioselective Formation of C-C bonds by Addition to Imines and Hydrazones: A Ten-year Update. *Chem. Rev.* **2011**, *111* (4), 2626–2704.
- (5) Nie, J.; Guo, H.-C.; Cahard, D.; Ma, J.-A. Asymmetric Construction of Stereogenic Carbon Centers Featuring a Trifluoromethyl Group from Prochiral Trifluoromethylated Substrates. *Chem. Rev.* **2011**, *111* (2), 455–529.
- (6) Candeias, N. R.; Montalbano, F.; Cal, P. M. S. D.; Gois, P. M. P. Boronic acids and esters in the Petasis-Borono Mannich Multi-component Reaction. *Chem. Rev.* **2010**, *110* (10), 6169–6193.
- (7) Handa, S.; Gnanadesikan, V.; Matsunaga, S.; Shibasaki, M. Heterobimetallic Transition Metal/Rate Earth Metal Bifunctional Catalysis: A Cu/Sm/Schiff Base Complex for Syn-Selective Catalytic Asymmetric Nitro-Mannich Reaction. *J. Am. Chem. Soc.* **2010**, *132* (13), 4925–4934.
- (8) Hashimoto, T.; Kimura, H.; Nakatsu, H.; Maruoka, K. Synthesis Application and Structural Elucidation of Axially Chiral Dicarboxylic Acid: Asymmetric Mannich-type Reaction with Diazoacetate, (Diazomethyl)phosphonate, and (Diazomethyl)sulfone. *J. Org. Chem.* **2011**, *76* (15), 6030–6037.
- (9) Colpaert, F.; Mangelinckx, S.; Kimpe, N. D. Asymmetric Synthesis of New Chiral β -Amino Acid Derivatives by Mannich-type Reactions of Chiral *N*-Sulfinyl Imidates with *N*-Tosyl Aldimines. *Org. Lett.* **2010**, *12* (9), 1904–1907.
- (10) Shibasaki, M.; Kanai, M. Asymmetric Synthesis of Tertiary Alcohols and α -Tertiary Amines via Cu-Catalyzed C-C Bond Formation to Ketones and Ketimines. *Chem. Rev.* **2008**, *108* (8), 2853–2873.
- (11) Lou, S.; Taoka, B. M.; Ting, A.; Schaus, S. E. Asymmetric Mannich Reactions of β -Keto Esters with Acyl Imines Catalyzed by Cinchona Alkaloids. *J. Am. Chem. Soc.* **2005**, *127* (32), 11256–11267.
- (12) Hayashi, W.; Tsuboi, W.; Ashimine, I.; Urushima, T.; Shoji, M.; Sakai, K. The Direct and Enantioselective, One-Pot, Three-Component, Cross-Mannich Reaction of Aldehydes. *Angew. Chem.* **2003**, *115*, 3805–3808.

- (13) Kobayashi, S.; Hamada, T.; Manabe, K. The Catalytic Asymmetric Mannich-type Reactions in Aqueous Media. *J. Am. Chem. Soc.* **2002**, *124* (20), 5640–5641.
- (14) Matsunaga, S.; Kumagai, N.; Harada, S.; Shibasaki, M. Anti-selective Direct Catalytic Asymmetric Mannich-type Reaction of Hydroxyketone providing β -Amino Alcohols. *J. Am. Chem. Soc.* **2003**, *125* (16), 4712–4713.
- (15) Zhang, H.; Mifsud, M.; Tanaka, F.; Barbas, C. F., III 3-Pyrrolidinecarboxylic Acid for Direct Catalytic Asymmetric anti-Mannich-Type Reactions of Unmodified Ketones. *J. Am. Chem. Soc.* **2006**, *128* (30), 9630–9631.
- (16) Córdova, A. The Direct Catalytic Asymmetric Mannich Reaction. *Acc. Chem. Res.* **2004**, *37* (2), 102–112.
- (17) Tramontini, M.; Angiolini, L.; Ghedini, N. Mannich Bases in Polymer Chemistry. *Polymer* **1988**, *29*, 771–788.
- (18) Roman, G. Mannich Bases in Medicinal Chemistry and Drug Design. *Eur. J. Med. Chem.* **2015**, *89*, 743–816.
- (19) Biersack, B.; Ahmed, K.; Padhye, S.; Schobert, R. Recent Developments Concerning the Application of the Mannich Reaction for Drug Design. *Expert Opin. Drug Discovery* **2018**, *13*, 39–49.
- (20) Karmakar, B.; Banerji, J. A Competent Pot and -Efficient Synthesis of Betti Bases over Nanocrystalline MgO involving a Modified Mannich Type Reaction. *Tetrahedron Lett.* **2011**, *52*, 4957–4960.
- (21) Kidwai, M.; Mishra, N. K.; Bansal, V.; Kumar, A.; Mozumdar, S. Novel One-Pot Cu-Nanoparticles-Catalyzed Mannich reaction. *Tetrahedron Lett.* **2009**, *50*, 1355–1358.
- (22) Ruan, S.-T.; Luo, J.-M.; Du, Y.; Huang, P.-Q. Asymmetric Vinylogous Mannich Reactions: A Versatile Approach to Functionalized Heterocycles. *Org. Lett.* **2011**, *13* (18), 4938–4941.
- (23) Ranieri, B.; Curti, C.; Battistini, L.; Sartori, A.; Pinna, L.; Casiraghi, G.; Zanardi, F. Diastereo- and Enantioselective Catalytic Vinylogous Mukaiyama-Mannich Reactions of Pyrrole-based Silyl Dienolates with Alkyl-substituted Aldehydes. *J. Org. Chem.* **2011**, *76* (24), 10291–10298.
- (24) Wang, C.-J.; Dong, X.-Q.; Zhang, Z.-H.; Xue, Z.-Y.; Teng, H.-L. Highly Anti-Selective Asymmetric Nitro-Mannich Reactions Catalyzed by Bifunctional Amine-Thiourea-Bearing Multiple Hydrogen-Bonding Donors. *J. Am. Chem. Soc.* **2008**, *130* (27), 8606–8607.
- (25) Leonard, N. J.; Klainer, J. A. Small charged rings. XIV. Dimer Formation through 2-arylaziridinium salts. *J. Heterocycl. Chem.* **1971**, *8*, 215–219.
- (26) Leonard, N. J.; Paukstelis, J. V. Direct Synthesis of Ternary Iminium Salts by Combination of Aldehyde or Ketones with Secondary Amine Salts. *J. Org. Chem.* **1963**, *28* (11), 3021–3024.
- (27) Ahond, A.; Cave, A.; Kan-Fan, C.; Husson, H.-P.; De Rostolan, J.; Potier, P. Facile N-O Bond Cleavages of Amine Oxides. *J. Am. Chem. Soc.* **1968**, *90*, 5622–5623.
- (28) Edward, J. T.; Whiting, J. Reactions of Amine Oxides and Hydroxylamines with Sulfur dioxide. *Can. J. Chem.* **1971**, *49*, 3502–3514.
- (29) Hwang, D.-R.; Uang, B.-J. A Modified Mannich-type Reaction Catalyzed by VO(acac)₂. *Org. Lett.* **2002**, *4* (3), 463–466.
- (30) Jin, Y.; Hu, Y.; Zhang, W. Tessellated Multiparous Two-Dimensional Covalent Organic Frameworks. *Nat. Rev. Chem.* **2017**, *1*, 0056.
- (31) Feng, X.; Ding, X.; Jiang, D. *Chem. Soc. Rev.* **2012**, *41*, 6010–6022.
- (32) Ding, S.-Y.; Wang, W. Covalent Organic Frameworks (COFs): From Design to Applications. *Chem. Soc. Rev.* **2013**, *42*, 548–568.
- (33) Bisbey, R. P.; Dichtel, W. R. Covalent Organic Frameworks as a Platform for Multidimensional Polymerization. *ACS Cent. Sci.* **2017**, *3* (6), 533–543.
- (34) Beuerle, F.; Gole, B. Covalent Organic Frameworks and Cage Compounds: Design and Applications of Polymeric and Discrete Organic Scaffolds. *Angew. Chem., Int. Ed.* **2018**, *57*, 4850–4878.
- (35) Das, S.; Heasman, P.; Ben, T.; Qui, S. Porous Organic Materials: Strategic Design and Structure-Function Correlation. *Chem. Rev.* **2017**, *117* (3), 1515–1563.
- (36) Diercks, C. S.; Yaghi, O. M. The Atom, The Molecule, and The Covalent Organic Framework. *Science* **2017**, *355*, No. eaal1585.
- (37) Slater, A. G.; Cooper, A. I. Function-led Design of New Porous Materials. *Science* **2015**, *348*, 988–998.
- (38) Waller, P. J.; Gandara, F.; Yaghi, O. M. Chemistry of Covalent Organic Frameworks. *Acc. Chem. Res.* **2015**, *48* (12), 3053–3063.
- (39) Huang, N.; Wang, P.; Jiang, D. Covalent Organic Frameworks: A Materials Platform for Structural and Functional Design. *Nat. Rev. Mater.* **2016**, *1*, 16068.
- (40) Diaz, U.; Corma, A. Ordered Covalent Organic Frameworks, COFs and PAFs. From Preparation to Application. *Coord. Chem. Rev.* **2016**, *311*, 85–124.
- (41) Lohse, M. S.; Bein, T. Covalent Organic Frameworks: Structure, Synthesis and Applications. *Adv. Funct. Mater.* **2018**, *28*, 1705553.
- (42) Côte, A. P.; Benin, A. I.; Ockwig, N. W.; O’Keeffe, M.; Matzger, A. J.; Yaghi, O. M. Porous, Crystalline, Covalent Organic Frameworks. *Science* **2005**, *310*, 1166–1170.
- (43) Pang, Z.-F.; Xu, S.-Q.; Zhou, T.-Y.; Liang, R.-R.; Zhan, T.-G.; Zhao, X. Construction of Covalent Organic Frameworks Bearing Three Different Kinds of Pores through the Heterostructural Mixed Linker Strategy. *J. Am. Chem. Soc.* **2016**, *138* (14), 4710–4713.
- (44) Rao, M. R.; Fang, Y.; De Feyter, S.; Perepichka, D. F. Conjugated Covalent Organic Frameworks via Michael Addition-Elimination. *J. Am. Chem. Soc.* **2017**, *139* (6), 2421–2427.
- (45) Lin, G.; Ding, H.; Yuan, D.; Wang, B.; Wang, C. A Pyrene-Based, Fluorescent Three-Dimensional Covalent Organic Framework. *J. Am. Chem. Soc.* **2016**, *138* (10), 3302–3305.
- (46) Kandambeth, S.; Mallick, A.; Lukose, B.; Mane, M. V.; Heine, T.; Banerjee, R. Construction of Crystalline 2D Covalent Organic Frameworks with Remarkable Chemical (Acid/Base) Stability via a Combined Reversible and Irreversible Route. *J. Am. Chem. Soc.* **2012**, *134* (48), 19524–19527.
- (47) Uribe-Romo, F. J.; Doonan, C. J.; Furukawa, H.; Oisaki, K.; Yaghi, O. M. Crystalline Covalent Organic Frameworks with Hydrazone Linkage. *J. Am. Chem. Soc.* **2011**, *133* (30), 11478–11481.
- (48) Ma, T.; Kapustin, E. A.; Yin, S. X.; Liang, L.; Zhou, Z.; Niu, J.; Li, H.; Wang, Y.; Su, J.; Li, J.; Wang, X.; Wang, W. D.; Wang, W.; Sun, J.; Yaghi, O. M. Single Crystal X-Ray Diffraction Structure of Covalent Organic Frameworks. *Science* **2018**, *361*, 48–52.
- (49) Zhang, J.; Han, X.; Wu, X.; Liu, Y.; Cui, Y. Multivariate Chiral Covalent Organic Frameworks with Controlled Crystallinity and Stability for Asymmetric Catalysis. *J. Am. Chem. Soc.* **2017**, *139* (24), 8277–8285.
- (50) Banerjee, T.; Haase, F.; Savasci, G.; Gottschling, K.; Ochsenfeld, C.; Lotsch, B. V. Single-site Photocatalytic H₂ Evolution from Covalent Organic Frameworks with Molecular Cobaloxime-Co-Catalysts. *J. Am. Chem. Soc.* **2017**, *139* (45), 16228–16234.
- (51) Lu, S.; Hu, Y.; Wan, S.; McCaffrey, R.; Jin, Y.; Gu, H.; Zhang, W. Synthesis of Ultrafine and Highly Dispersed Metal Nanoparticles Confined in a Thioether-Containing Covalent Organic Framework and their Catalytic Application. *J. Am. Chem. Soc.* **2017**, *139* (47), 17082–17088.
- (52) Diercks, C. S.; Lin, S.; Kornienko, N.; Kapustin, E. A.; Nichols, E. M.; Zhu, C.; Zhao, Y.; Chang, C. J.; Yaghi, O. M. Reticular Electronic Tuning of Porphyrin Active Sites in Covalent Organic Frameworks for Electrocatalytic Carbon dioxide Reduction. *J. Am. Chem. Soc.* **2018**, *140* (3), 1116–1122.
- (53) Han, X.; Xia, Q.; Huang, J.; Liu, Y.; Tan, C.; Cui, Y. Chiral Covalent Organic Frameworks with High Chemical Stability for Heterogeneous Asymmetric Catalysis. *J. Am. Chem. Soc.* **2017**, *139* (25), 8693–8697.
- (54) Pachfule, P.; Acharjya, A.; Roeser, J.; Langenhahn, T.; Schwarze, M.; Schomacker, R.; Thomas, A.; Schmidt, J. Diacetylene Functionalized Covalent Organic Framework (COF) for Photocatalytic Hydrogen Generation. *J. Am. Chem. Soc.* **2018**, *140* (4), 1423–1427.
- (55) Wei, P.-F.; Qi, M.-Z.; Wang, Z.-P.; Ding, S.-Y.; Yu, W.; Liu, Q.; Wang, L.-K.; Wang, H.-Z.; An, W.-K.; Wang, W. Benzoxazole-linked Ultrastable Covalent Organic Frameworks for Photocatalysis. *J. Am. Chem. Soc.* **2018**, *140* (13), 4623–4631.

- (56) Sick, T.; Hufnagel, A. G.; Kampmann, J.; Kondofersky, I.; Calik, M.; Rotter, J. M.; Evans, A.; Dobliger, M.; Herbert, S.; Peters, K.; Bohm, D.; Knochel, P.; Medina, D. D.; Fattakhova-Rohlfing, D.; Bein, T. Oriented films of Conjugated 2D Covalent Organic Frameworks as Photocathodes for Water Splitting. *J. Am. Chem. Soc.* **2018**, *140* (6), 2085–2092.
- (57) Lin, S.; Diercks, C. S.; Zhang, Y.-B.; Kornienko, N.; Nichols, E. M.; Zhao, Y.; Paris, A. R.; Kim, D.; Yang, P.; Yaghi, O. M.; Chang, C. J. Covalent Organic Frameworks Comprising for Catalytic CO₂ Reduction in Water. *Science* **2015**, *349*, 1208–1213.
- (58) Ding, S.-Y.; Gao, J.; Wang, Q.; Zhang, Y.; Song, W.-G.; Su, C.-Y.; Wang, W. Construction of Covalent Organic Framework for Catalysis: Pd/COF-LZU 1 in Suzuki-Miyaura Coupling Reaction. *J. Am. Chem. Soc.* **2011**, *133* (49), 19816–19822.
- (59) Sun, Q.; Aguila, B.; Ma, S. Bifunctional Covalent Organic Framework as an Efficient Platform for Cascade Catalysis. *Mater. Chem. Front.* **2017**, *1*, 1310–1316.
- (60) Sun, Q.; Aguila, B.; Perman, J. A.; Nguyen, N.; Ma, S. Flexibility Matters: Cooperation Active Sites in Covalent Organic Framework and Threaded Ionic Polymer. *J. Am. Chem. Soc.* **2016**, *138* (48), 15790–15796.
- (61) Wang, X.; Han, X.; Zhang, J.; Wu, X.; Liu, Y.; Cui, Y. Homochiral 2D Porous Covalent organic Frameworks for Heterogeneous Asymmetric Catalysis. *J. Am. Chem. Soc.* **2016**, *138* (38), 12332–12335.
- (62) Du, Y.; Yang, H.; Whiteley, J. M.; Wan, S.; Jin, Y.; Lee, S.-H.; Zhang, W. Ionic Covalent Organic Frameworks with Spiroborate Linkage. *Angew. Chem., Int. Ed.* **2016**, *55*, 1737–1741.
- (63) Doonan, C. J.; Tranchemontagne, D. J.; Glover, T. G.; Hunt, J. R.; Yaghi, O. M. Exceptional Ammonia Uptake by a Covalent Organic Framework. *Nat. Chem.* **2010**, *2*, 235–238.
- (64) Zeng, Y.; Zou, R.; Zhao, Y. Covalent Organic Frameworks for CO₂ Capture. *Adv. Mater.* **2016**, *28*, 2855–2873.
- (65) Baldwin, L. A.; Crowe, J. W.; Pyles, D. A.; McGrier, P. L. Metalation of a Mesoporous Three-Dimensional Covalent Organic Framework. *J. Am. Chem. Soc.* **2016**, *138* (46), 15134–15137.
- (66) Pramudya, Y.; Mendoza-Cortes, J. L. Design Principles for High H₂ Storage using Chelation of Abundant Transition Metals in Covalent Organic Frameworks for 0–700 bar at 298 K. *J. Am. Chem. Soc.* **2016**, *138* (46), 15204–15213.
- (67) Yang, Y.; Faheem, M.; Wang, L.; Meng, Q.; Sha, H.; Yang, N.; Yuan, Y.; Zhu, G. Surface Pore Engineering of Covalent Organic Frameworks for Ammonia Capture through Synergistic Multivariate and Open Metal Site Approached. *ACS Cent. Sci.* **2018**, *4* (6), 748–754.
- (68) Sun, Q.; Aguila, B.; Perman, J.; Earl, L.; Abney, C.; Cheng, Y.; Wei, H.; Nguyen, N.; Wojtas, L.; Ma, S. Postsynthetically Modified Covalent Organic Frameworks for Efficient and Effective Mercury Removal. *J. Am. Chem. Soc.* **2017**, *139* (7), 2786–2793.
- (69) Sun, Q.; Aguila, B.; Earl, L. D.; Abney, C. W.; Wojtas, L.; Thallapally, P. K.; Ma, S. Covalent Organic Frameworks as a Decorating Platform for Utilization and Affinity Enhancement of Chelating Sites for Radionuclide Sequestration. *Adv. Mater.* **2018**, *30*, 1705479.
- (70) Bertrand, G. H. V.; Michaelis, V. K.; Ong, T.-C.; Griffin, R. G.; Dincă, M. Thiophene-based Covalent Organic Frameworks. *Proc. Natl. Acad. Sci. U. S. A.* **2013**, *110*, 4923–4928.
- (71) Calik, M.; Auras, F.; Salonen, L. M.; Bader, K.; Grill, I.; Handloser, M.; Medina, D. D.; Dogru, M.; Löbermann, F.; Trauner, D.; Hartschuh, A.; Bein, T. Extraction of Photogenerated Electrons and Holes from a Covalent Organic Framework Integrated Heterojunction. *J. Am. Chem. Soc.* **2014**, *136* (51), 17802–17807.
- (72) Chen, L.; Furukawa, K.; Gao, J.; Nagai, A.; Nakamura, T.; Dong, Y.; Jiang, D. Photoelectric Covalent Organic Frameworks: Converting Open Lattices into Ordered Donor-Acceptor Heterojunctions. *J. Am. Chem. Soc.* **2014**, *136* (28), 9806–9809.
- (73) Ma, H.; Liu, B.; Li, B.; Zhang, L.; Li, Y.-G.; Tan, H.-Q.; Zang, H.-Y.; Zhu, G. Cationic Covalent Organic Frameworks: A Simple Platform of Anionic Exchange for Porosity Tuning and Proton Conduction. *J. Am. Chem. Soc.* **2016**, *138* (18), 5897–5903.
- (74) Fang, Q.; Wang, J.; Gu, S.; Kaspar, R. B.; Zhuang, Z.; Zheng, J.; Guo, H.; Qiu, S.; Yan, Y. 3D Porous Crystalline Polyimide Covalent Organic Frameworks for Drug Delivery. *J. Am. Chem. Soc.* **2015**, *137* (26), 8352–8355.
- (75) Kandambeth, S.; Venkatesh, V.; Shinde, D. B.; Kumari, S.; Halder, A.; Verma, S.; Banerjee, R. Self-templated Chemically Stable Hollow Spherical Covalent Organic Framework. *Nat. Commun.* **2015**, *6*, 6786.
- (76) Wang, S.; Wang, Q.; Shao, P.; Han, Y.; Gao, X.; Ma, L.; Yuan, S.; Ma, X.; Zhou, J.; Feng, X.; Wang, B. Exfoliation of Covalent Organic frameworks into Few-Layer Redox-Active Nanosheets as Cathode Materials for Lithium-Ion Batteries. *J. Am. Chem. Soc.* **2017**, *139* (12), 4258–4261.
- (77) Ning, G.-H.; Chen, Z.; Gao, Q.; Tang, W.; Chen, Z.; Liu, C.; Tian, B.; Li, X.; Loh, K. P. Salicylideneanilines-Based Covalent Organic Frameworks as Chemoselective Molecular Sieves. *J. Am. Chem. Soc.* **2017**, *139* (26), 8897–8904.
- (78) Peng, Y.; Huang, Y.; Zhu, Y.; Chen, B.; Wang, L.; Lai, Z.; Zhang, Z.; Zhao, M.; Tan, C.; Yang, N.; Shao, F.; Han, Y.; Zhang, H. Ultrathin Two-Dimensional Covalent Organic Framework Nanosheets: Preparation and Application in Highly Sensitive and Selective DNA Detection. *J. Am. Chem. Soc.* **2017**, *139* (25), 8698–8704.
- (79) Zhang, S.; Zheng, Y.; An, H.; Aguila, B.; Yang, C.-X.; Dong, Y.; Xie, W.; Cheng, P.; Zhang, Z.; Chen, Y.; Ma, S. Covalent Organic Frameworks with Chirality Enriched by Biomolecules for Efficient Chiral Separation. *Angew. Chem., Int. Ed.* **2018**, *57*, 16754–16759.
- (80) Sun, Q.; Aguila, B.; Perman, J.; Butts, T.; Xiao, F.-S.; Ma, S. Integrating Superwettability within Covalent Organic Frameworks for Functional Coating. *Chem.* **2018**, *4*, 1726–1739.
- (81) Han, X.; Huang, J.; Yuan, C.; Liu, Y.; Cui, J. Chiral 3D Covalent Organic Frameworks for High Performance Liquid Chromatographic Enantioseparation. *J. Am. Chem. Soc.* **2018**, *140* (3), 892–895.
- (82) Mitra, S.; Sasmal, H. S.; Kundu, T.; Kandambeth, S.; Illath, K.; Diaz Diaz, D.; Banerjee, R. Targeted Drug Delivery in Covalent Organic Nanosheets (CONs) via Sequential Postsynthetic Modification. *J. Am. Chem. Soc.* **2017**, *139* (12), 4513–4520.
- (83) Mal, A.; Mishra, R. K.; Praveen, V. K.; Khayum, M. A.; Banerjee, R.; Ajayaghosh, A. Supramolecular Reassembly of Self-exfoliated Ionic Covalent Organic Nanosheets for Label-free Detection of Double-stranded DNA. *Angew. Chem., Int. Ed.* **2018**, *57*, 8443–8447.
- (84) Mulzer, C. R.; Shen, L.; Bisbey, R. P.; McKone, J. R.; Zhang, N.; Abruna, H. D.; Dichtel, W. R. Superior Charge Storage and Power Density of a Conducting Polymer-Modified Covalent Organic Framework. *ACS Cent. Sci.* **2016**, *2* (9), 667–673.
- (85) Lin, C.-Y.; Zhang, D.; Zhao, Z.; Xia, Z. Covalent Organic Framework Electrocatalysts for Clean Energy Conversion. *Adv. Mater.* **2018**, *30*, 1703646.
- (86) Song, Y.; Sun, Q.; Aguila, B.; Ma, S. Opportunities of Covalent Organic Frameworks for Advanced Applications. *Adv. Sci.* **2019**, *6*, 1801410.
- (87) Waller, P. J.; Alfaraj, Y. S.; Diercks, C. S.; Jarenwattananon, N. N.; Yaghi, O. M. Conversion of Imine to Oxazole and Thiazole Linkages in Covalent Organic Frameworks. *J. Am. Chem. Soc.* **2018**, *140* (29), 9099–9103.
- (88) Halder, A.; Ghosh, M.; Khayum, A.; Bera, S.; Addicoat, M.; Sasmal, H. S.; Karak, S.; Kurungot, S.; Banerjee, R. Interlayer Hydrogen-bonded Covalent Organic Frameworks as High-Performance Supercapacitors. *J. Am. Chem. Soc.* **2018**, *140* (35), 10941–10945.
- (89) Vardhan, H.; Verma, G.; Ramani, S.; Nafady, A.; Al-Enizi, A.; Pan, Y.; Yang, Z.; Yang, H.; Ma, S. Covalent Organic Framework Decorated with Vanadium as a New Platform for Prins Reaction and Sulphide Oxidation. *ACS Appl. Mater. Interfaces* **2019**, *11* (3), 3070–3079.
- (90) Cooper, S. R.; Koh, Y. B.; Raymond, K. N. Synthesis, Structural, and Physical Studies of Bis(triethylammonium)Tris(catecholato)-vanadate(IV), Potassium Bis(catcholato)oxovanadate(IV), and Potas-

sium Tris(catecholato)vanadate(III). *J. Am. Chem. Soc.* **1982**, *104* (19), 5092–5102.

(91) Grudziński, K.; Malinska, M.; Barbasiewicz, M. Synthesis and Properties of bimetallic Hoveyda-Grubbs Metathesis catalysts. *Organometallics* **2012**, *31* (9), 3636–3646.

(92) Huang, N.; Wang, P.; Addicoat, M. A.; Heine, T.; Jiang, D. Ionic Covalent Organic Frameworks: Design of a Charged Interface Aligned on 1D Channel Walls and Its Unusual Electrostatic Functions. *Angew. Chem., Int. Ed.* **2017**, *56*, 4982–4986.

(93) Gomes, R.; Bhanja, P.; Bhaumik, A. A Triazine-based Covalent Organic Polymer for Efficient CO₂ Adsorption. *Chem. Commun.* **2015**, *51*, 10050–10053.

(94) Halder, A.; Kandambeth, S.; Biswal, B. P.; Kaur, G.; Roy, N. C.; Addicoat, M.; Salunke, J. K.; Banerjee, S.; Vanka, K.; Heine, T.; Verma, S.; Banerjee, R. Decoding the Morphological Diversity in Two Dimensional Crystalline Porous Polymers by Core Planarity Modulation. *Angew. Chem., Int. Ed.* **2016**, *55*, 7806–7810.

(95) Chen, X.; Huang, N.; Gao, J.; Xu, H.; Xu, F.; Jiang, D. Towards Covalent Organic Frameworks with Pre-designable and Aligned Open Docking Sites. *Chem. Commun.* **2014**, *50*, 6161–6163.

(96) Sun, Q.; Fu, C.-W.; Aguila, B.; Perman, J.; Wang, S.; Huang, H.-Y.; Xiao, F.-S.; Ma, S. Pore Environment Control and Enhanced Performance of Enzymes Infiltrated in Covalent Organic Frameworks. *J. Am. Chem. Soc.* **2018**, *140* (3), 984–992.

(97) Lu, Q.; Ma, Y.; Li, H.; Guan, X.; Yusran, Y.; Xue, M.; Fang, Q.; Yan, Y.; Qiu, S.; Valtchev, V. Post Synthetic Functionalization of Three-dimensional Covalent Organic Frameworks for Selective Extraction of Lanthanide Ions. *Angew. Chem., Int. Ed.* **2018**, *57*, 6042–6048.

(98) Leng, W.; Peng, Y.; Zhang, J.; Lu, H.; Xiao, F.; Ge, R.; Dong, B.; Wang, B.; Hu, X.; Gao, Y. Sophisticated Design of Covalent Organic Frameworks with Controllable Bimetallic Docking for a Cascade Reaction. *Chem. - Eur. J.* **2016**, *22*, 9087–9091.

(99) Maurya, M. R.; Kumar, U.; Manikandan, P. Polymer Supported Vanadium and Molybdenum Complexes as Potential Catalysts for the Oxidation and Oxidative Bromination of Organic Substrates. *Dalton Trans.* **2006**, 3561–3575.

(100) Jena, H. S.; Krishnaraj, C.; Wang, G.; Leus, K.; Schmidt, J.; Chaoui, N.; Van Der Voort, P. Acetylacetone Covalent Triazine Framework: An Efficient Carbon Capture and Storage Material and a Highly Stable Heterogeneous Catalyst. *Chem. Mater.* **2018**, *30* (12), 4102–4111.

(101) Langeslay, R. R.; Kaphan, D. M.; Marshall, C. L.; Stair, P. C.; Sattelberger, A. P.; Delferro, M. Catalytic Application of Vanadium: A Mechanistic Perspective. DOI: *Chem. Rev.* **2018** DOI: [10.1021/acs.chemrev.8b00245](https://doi.org/10.1021/acs.chemrev.8b00245).

(102) Zhu, L.; Liu, X.-Q.; Jiang, H.-L.; Sun, L.-B. Metal-Organic Frameworks for Heterogeneous Basic Catalysis. *Chem. Rev.* **2017**, *117* (12), 8129–8176.

(103) Furukawa, H.; Aguila, B.; Sun, Q.; Wang, X.; O'Rourke, E.; Al-Enizi, A. M.; Nafady, A.; Ma, S. Lower Activation Energy for Catalytic Reactions through Host-Guest Cooperation within Metal-Organic Frameworks. *Angew. Chem., Int. Ed.* **2018**, *57*, 10107–10111.

(104) Dhakshinamoorthy, A.; Garcia, H. Cascade Reactions Catalyzed by Metal-Organic Frameworks. *ChemSusChem* **2014**, *7*, 2392–2410.

(105) Niu, Z.; Gunatilleke, W. D. C. B.; Sun, Q.; Lan, P. C.; Perman, J.; Ma, J.-G.; Cheng, Y.; Aguila, B.; Ma, S. Metal-Organic Framework Anchored with Lewis Pair as a New Paradigm for Catalysis. *Chem.* **2018**, *4*, 2587–2599.

(106) Farrusseng, D.; Aguado, S.; Pinel, C. Metal-Organic frameworks: Opportunities for Catalysis. *Angew. Chem., Int. Ed.* **2009**, *48*, 7502–7513.

(107) Dhakshinamoorthy, A.; Asiri, A. M.; Garcia, H. Metal-Organic Frameworks Catalyzed C-C and C-Heteroatom Coupling Reactions. *Chem. Soc. Rev.* **2015**, *44*, 1922–1947.